

The East Gotland Basin (Baltic Sea) as a candidate Global Boundary Stratotype Section and Point for the Anthropocene series

The Anthropocene Review

1–24

© The Author(s) 2022



Article reuse guidelines:

sagepub.com/journals-permissions

DOI: 10.1177/20530196221132709

journals.sagepub.com/home/anr

Jérôme Kaiser,^{1*}  Serena Abel,^{2§} Helge W Arz,^{1§}
Andrew B Cundy,^{3§} Olaf Dellwig,^{1§} Pawel Gaca,^{3§}
Gunnar Gerdts,^{2§} Irka Hajdas,^{4§}  Matthias Labrenz,^{1§}
James A Milton,^{3§} Matthias Moros,^{1§}
Sebastian Pimpke,^{2§} Sarah L Roberts,^{5§} Neil L Rose,^{5§}
Simon D Turner,^{5§} Maren Voss^{1§}
and Juliana A Ivar do Sul^{1*} 

Abstract

The short sediment core EMB201/7-4 retrieved from the East Gotland Basin, central Baltic Sea, is explored here as a candidate to host the stratigraphical basis for the Anthropocene series and its equivalent Anthropocene epoch, still to be formalized in the Geological Time Scale. The core has been accurately dated back to 1840 CE using a well-established event stratigraphy approach. A pronounced and significant change occurs at 26.5 cm (dated 1956 ± 4 CE) for a range of geochemical markers including ²³⁹⁺²⁴⁰Pu, ²⁴¹Am, fly-ash particles, DDT (organochlorine insecticide), total organic carbon, and bulk organic carbon stable isotopes. This stratigraphic level, which corresponds to a change in both lithology and sediment colour related to early anthropogenic-triggered eutrophication of the central Baltic Sea, is proposed as a Global Boundary Stratotype Section and Point for the Anthropocene series.

Keywords

anoxic marine basin, biomarkers, eutrophication, GSSP, microplastics, organic-rich sediments, radiocarbon, radionuclides, SCPs

¹Leibniz Institute for Baltic Sea Research Warnemünde (IOW), Germany

²Alfred Wegener Institute (AWI), Helmholtz Centre for Polar and Marine Research, Germany

³University of Southampton, UK

⁴ETH Zurich, Switzerland

⁵University College London, UK

*These authors contributed equally to the manuscript.

§Authors listed in alphabetical order.

Corresponding author:

Jérôme Kaiser, Leibniz Institute for Baltic Sea Research (IOW), Marine Geology, Seestrasse 15, 18119 Rostock-Warnemünde, Germany.

Email: jerome.kaiser@io-warnemuende.de

Introduction

Semi-enclosed basins such as the Baltic Sea are highly impacted by anthropogenic pressures in their catchment areas. Well-known consequences of human-driven eutrophication impacts on the Baltic Sea ecosystem are water deoxygenation and the spread of hypoxic or 'dead' zones in deep basins and coastal areas (Andersen et al., 2017; Carstensen et al., 2014; Gustafsson et al., 2012; Reusch et al., 2018). Eutrophication is defined as the enrichment of water by nutrients (nitrogen, phosphorus), which causes an accelerated growth of algae and plants that produce an undesirable disturbance in the balance of organisms present in the water and to the quality of the water concerned (OSPAR, 1998). It reduces the amount of oxygen in water due to the decomposition of sinking organic material by oxygen consuming bacteria, and can eventually lead to benthic ecosystem collapses.

Because of eutrophication, the East Gotland Basin (EGB; 249 m water depth at its deepest point), located in the central Baltic Sea, has been almost permanently hypoxic below 80 m (i.e. water oxygen concentration $<2 \text{ ml l}^{-1}$) since the 1950s, and even euxinic in its deepest part (Carstensen et al., 2014; Gustafsson et al., 2012). The expansion of oxygen deficient bottom waters in the central Baltic Sea is interrupted for a few months only during Major Baltic Inflows (MBIs), which are intrusions of oxygen-rich waters from the North Sea (Dellwig et al., 2018; Mohrholz, 2018). MBIs are occasional and occur only when long-lasting easterly winds causing a below-normal Baltic sea level are followed by strong westerly winds (Mohrholz et al., 2015). These inflow events are recorded in sediments through the formation of Mn carbonate (or Ca-rich rhodochrosite) and/or through significant increase in specific trace metals such as Co and V (Dellwig et al., 2019, 2021). Except for these mm-thick Mn carbonate-rich layers, a hemipelagic-type of sedimentation with a high content of organic carbon (5%–18%) and relatively high sedimentation rates ($0.3\text{--}0.5 \text{ cm yr}^{-1}$) has prevailed in the EGB since 1950 CE (Ilus et al., 2007; Kaiser et al., 2020; Lin et al., 2021; Struck et al., 2001). The mean sinking velocity of particles (diatoms) has been estimated around $15 \text{ to } 70 \text{ m d}^{-1}$ (Passow, 1991), which means a particle at the sea surface needs 3 to 16 days to reach the seabed of the EGB. Anoxic conditions in bottom waters of the EGB prevent benthic colonization and bioturbation, and enable the formation of mm-scale laminated sediments in an undisturbed stratigraphic sequence after 1950 CE (Ilus et al., 2007). In contrast to annually or seasonally laminated lake sediments, multiple laminations in Baltic Sea sediments are not annual but controlled by several factors so the composition of single laminae also varies (Brenner, 2001; Lepland and Stevens, 1998; Sohlenius and Westman, 1998). Before the mid-20th century, the sediment is grey, homogeneous and silty-clayey. Recent sediments (<180 years) from the EGB are thus well-suited to record precisely and continuously the natural and anthropogenic development of the Baltic Sea and its catchment area. Here, we show that the Baltic Sea represents a high quality candidate to host the onset of the Anthropocene via selection of a Global boundary Stratotype Section and Point (GSSP) for the base of the Anthropocene, that would comprise both a geochronological unit (an Anthropocene epoch) and a chronostratigraphic unit (an Anthropocene series) (Head et al., 2021). The preparatory activities of the Anthropocene Working Group, including events leading to the submission of GSSP proposals and the binding decision that the base of the Anthropocene should align with stratigraphic signals dating to the mid-20th century, are detailed in the introductory article to this special issue (Waters et al., in submission).

Materials and methods

Geographic settings

The Baltic Sea, the world second largest brackish sea, is a shallow, marginal sea with a mean depth of 55 m, and is characterized by an estuarine-like circulation (Elken and Matthäus, 2008). The upper water layer (0–60 m) has low salinities ($7\text{--}8 \text{ g kg}^{-1}$) caused by high freshwater inputs by

rivers in the eastern and northern parts of the drainage basin. As a counterpart, relatively high saline water from the North Sea flows in through the Danish Straits. This dense water spreads into deep layers and causes a strong vertical salinity gradient in the central Baltic Sea, with a pronounced halocline around 60–80 m depth. The inflow of saline waters is balanced by upwelling, diapycnal mixing and the outflow of brackish water in surface layers. The catchment area of the Baltic Sea covers 1.7 million km², that is more than four times the area of the Baltic Sea itself (369,000 km²), and is drained by >200 rivers (Håkanson et al., 2003; Snoeijs-Leijonmalm and Andrén, 2017). About 85 million people live within the Baltic Sea catchment area, and 18% of them within 10 km of the coast (HELCOM, 2010). Agriculture land areas are concentrated mainly in the southern part of the drainage basin, where they occupy >65% of the land area (Snoeijs-Leijonmalm and Andrén, 2017).

Field collection, core scanning, and sampling

Sediment core EMB201/7-4 (57°16.980'N, 020°07.228'E; 241 m water depth; Figure 1) was recovered from the EGB on December 6, 2018, during expedition EMB201 on board the research vessel Elisabeth Mann Borgese. The coring site was located in the exclusive economic zone of Latvia. A multicorer, equipped with 60 cm-long polyvinyl chloride tubes, was used as this coring device keeps the water-sediment interface undisturbed. The 45 cm-long core was opened lengthwise on board and kept refrigerated (4°C) in the core repository of the Leibniz Institute for Baltic Sea Research (IOW, Germany). Both core halves were scanned at the IOW with an ITRAX X-ray fluorescence (XRF) scanner (Cox Analytical Systems) equipped with a Cr tube operated at 30 kV and 55 mA (exposure time of 5 s) with a 200 µm resolution (Supplemental Table S1). X-ray radiography was recorded at 60 kV and 30 mA, with an exposure time of 225 ms, and at a 200 µm resolution, to identify variations in density along the sediment core. In June 2020, one half of the sediment core was sampled at the IOW in an enclosed laminar flow workstation to prevent airborne contamination. Due to the high water content of recent sediments in the upper part of the core, and to guarantee sufficient amount of sediments for all analyses, the sampling strategy included slicing the core every 1 cm from 0 to 27 cm depth, and every 0.5 cm from 27 to 45 cm depth. This resulted in a total of 63 samples, which were freeze-dried and homogenized before analysis. The second half of the core is kept in the IOW repository as an archive.

Chronological control

An event stratigraphy approach has been developed to accurately date Baltic Sea recent sediments (Dellwig et al., 2018, 2021; Kaiser et al., 2020; Lin et al., 2021). This method was applied with modifications in the present study to establish the age model of core EMB201/7-4. Artificial radionuclides (²³⁹⁺²⁴⁰Pu, ²⁴¹Am, ¹³⁷Cs) here were not used as time markers, but as Anthropocene proxies, except ¹³⁷Cs for the Chernobyl accident in 1986 (see below).

Anthropocene proxies

Relevant proxies used to define the onset of the Anthropocene epoch follow recommendations from Zalasiewicz et al. (2019).

²⁴¹Am, ¹³⁷Cs and ²¹⁰Pb. Artificial radionuclides ²¹⁰Am, ¹³⁷Cs and natural ²¹⁰Pb were analysed at the IOW, Germany, by gamma spectrometry with a Ge-well detector (GCW4021-7500SL-RDC-6-ULB). Raw data were then processed with the GENIE 2000 software (Canberra Industries Inc.,

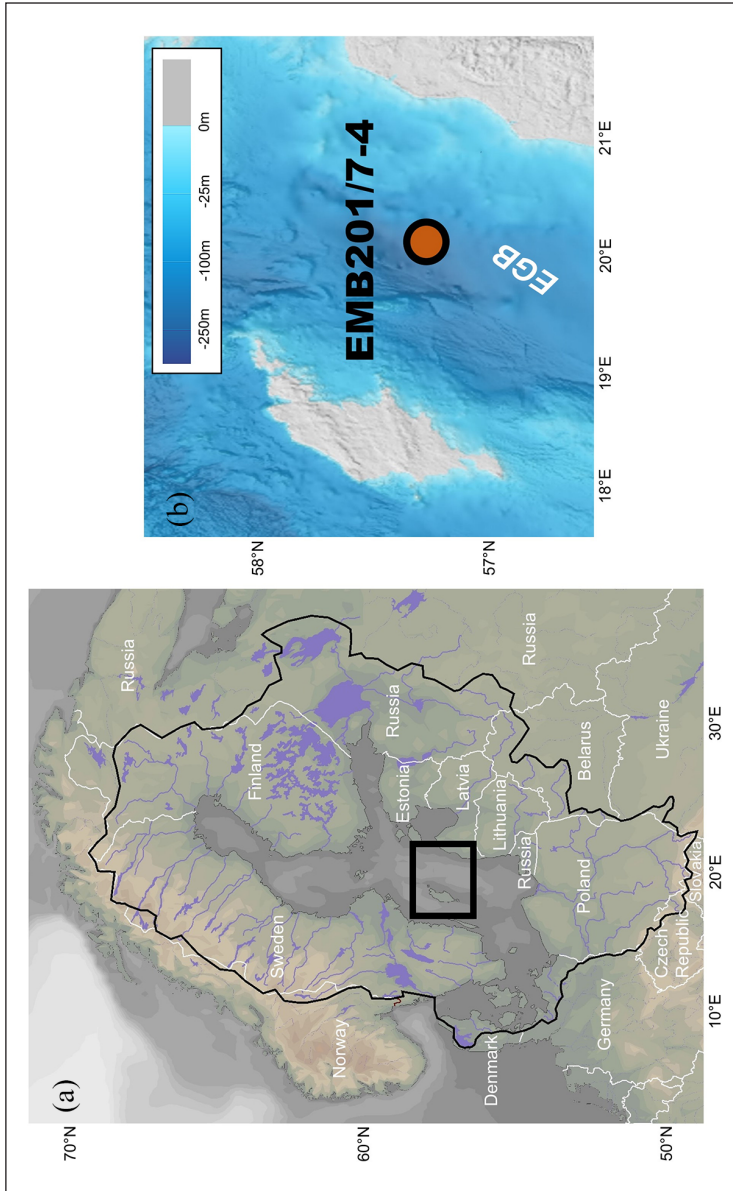


Figure 1. (a) Study area (black rectangle) in the Baltic Sea; the countries, main lakes and rivers of the catchment area – delimited by a bold line – are shown; (b) bathymetric chart (Baltic Sea Bathymetry Database) of the study area with the location of core EMB201/7-4 in the East Gotland Basin (EGB).

USA). Counting statistics were better than 5%–10% for ^{210}Pb and ^{137}Cs and better than 20% for ^{241}Am activities, respectively. The radionuclide activities were calculated using the following standard reference materials (decay corrected): IAEA-447 (^{137}Cs , ^{210}Pb , ^{226}Ra), IAEA-384 (^{241}Am) and IAEA-385 (^{241}Am , ^{137}Cs , ^{226}Ra). The energies used for quantification of isotopes were 46.5 keV for ^{210}Pb , 295 keV and 351 keV for ^{226}Ra , 59.5 keV for ^{241}Am , and 661 keV for ^{137}Cs (Moros et al., 2017). A total of 49 samples was analysed, that is all samples between 0 and 31.5 cm and every second sample between 32 and 44.5 cm (Supplemental Table S2).

^{238}Pu , ^{239}Pu and ^{240}Pu . Pu isotopes were analysed at the GAU-Radioanalytical Laboratories of the University of Southampton, UK. Briefly, sediment samples ($n=20$; Supplemental Table S2) were transferred to glass beakers and ignited at 450°C to remove organic matter. The remaining inorganic fraction was spiked with ^{242}Pu chemical recovery tracer, mixed with lithium metaborate flux and fused at 1100°C to achieve a homogeneous melt. The obtained liquid glass was then quenched in deionised water and the resulting solidified glass was dissolved in 8M HNO_3 at 90°C (overnight). The resulting solution was cooled to room temperature and the precipitated boric acid, resulting from the added flux, was filtered off using a GF/A filter paper. Pu was pre-concentrated from the sample solution by means of co-precipitation with $\text{Fe}(\text{OH})_3$ at pH 5–6. The precipitate was separated by centrifuging and re-dissolved in 9M HCl. These solutions were transferred to anion exchange columns, previously pre-conditioned with 9M HCl. Pu was retained on the columns and was purified by sequential washes with 9M HCl, 8M HNO_3 and again with 9M HCl. Finally, the Pu fraction was eluted to pre-cleaned beakers using 0.1M $\text{NH}_4\text{I}/9\text{M}$ HCl solution. The solution was evaporated to dryness with HNO_3 added to remove excess iodine present and thin alpha spectrometric sources were prepared by electrodeposition. Each source was then counted using Octete (Ortec/Amtek) alpha spectrometers equipped with passivated implanted planar silicon (PIPS) detectors. The resulting spectra were analysed using Maestro spectral analysis software. Following counting, $^{240}\text{Pu}/^{239}\text{Pu}$ ratios were determined using a Thermo Scientific Neptune Plus MC-ICP-MS after radiochemical re-purification of the Pu alpha spectrometry discs (Łokas et al., 2022).

Radiocarbon (^{14}C). ^{14}C was analysed by accelerator mass spectrometry (AMS) at the ETH Zürich, Switzerland. Sediment samples ($n=20$; Supplemental Table S2) were selected between 1 and 31 cm depth, where the highest ^{14}C activity was expected. Each sample (0.1–0.3 g) was subject to acid-base-acid treatment (Hajdas, 2008; Hajdas et al., 2021). Briefly, in the first acid step bulk sediment was decarbonated with 0.5M HCl to remove inorganic carbon. After a washing to neutral with MilliQ water the decarbonated sediment was treated with 0.1M NaOH. The liquid was extracted and a few ml of 0.5M HCl were added to precipitate the base-extracted organic fraction (or humic acid fraction), and freeze dried. The residue, that is, the base-insoluble organic fraction (or humin fraction), was washed to neutral, treated with 0.5M HCl, washed again to neutral, and freeze-dried. Both fractions were weighed into Al cups for combustion in an elemental analyser (Vario Micro Cube; Elementar) and subsequent graphitization (Němec et al., 2010). The graphite powder was pressed into the Al cathodes to measure $^{14}\text{C}/^{12}\text{C}$ and $^{13}\text{C}/^{12}\text{C}$ ratios using the AMS system of MICADAS (Synal et al., 2000; Wacker et al., 2010). Results are reported as fraction modern F^{14}C (Reimer et al., 2004) and radiocarbon ages (Before Present, BP, where 0 BP = 1950 CE; (Stuiver and Polach, 1977). For an overview of the method and data reporting see Hajdas et al. (2021).

Fly-ash. Spheroidal carbonaceous fly-ash particles (SCPs) were analysed at University College London, UK (Rose, 1994). Briefly, sediments (0.2 g; $n=52$; Supplemental Table S2) were subjected to sequential chemical attack by mineral acids to remove unwanted fractions leaving a

suspension of mainly carbonaceous material in water. A known fraction of this final suspension was evaporated onto a coverslip and mounted onto a microscope slide. SCPs were then counted using a light microscope at x450 magnification and the sediment content calculated in units of SCPs per gram of sediment dry weight (SCPs g^{-1} dw). The criteria for SCP identification under the light microscope followed (Rose, 2008). The detection limit for the technique is typically ca. 100 SCPs g^{-1} dw and accuracy is ca. ± 45 SCPs g^{-1} dw (Rose, 2008) although detection limits were slightly higher in this core (ca. 300 SCPs g^{-1} dw). SCPs were sub-divided into size classes during counting. Analytical blanks and SCP reference material were included in duplicate and triplicate, respectively. Reference materials agreed closely with expected values (6005 ± 70 SCPs g^{-1} dw), while no SCPs were observed in blanks. SCPs were not analysed between 2 and 9 cm due to the low amount of available sediment.

Microplastics. Microplastics (MPs) sampling strategy aimed to maximize MP particles recovery by merging consecutive layers in the core to reach a minimum of ca. 1 g sediment dw, resulting in a total of 20 samples (Supplemental Table S2). Potential MPs (particle size between 11 μm and 5 mm) were extracted and isolated from sediments at the IOW, Germany, following a well-established protocol (Enders et al., 2020). Briefly, sediments were submitted to a density separation by using sodium polytungstate (1800 kg m^{-3}), which allows all plastic particles to float, and digested with 30% H_2O_2 to eliminate organic particles. The method recovery rate has been estimated to 80%. Automated particle-based analysis was performed at the Biological Institute Helgoland (BAH) of the Alfred Wegener Institute, Helmholtz Centre for Polar and Marine Research, Germany, following a well-established protocol (Primpke et al., 2018). Purified samples were submitted to a second density separation and digestion steps (Abel et al., 2021) to disaggregate flocculates and eliminate potential biofilm immediately before micro-Fourier transform infrared spectroscopic analysis (μFTIR ; Hyperion 3000m, Bunker Optics GmbH). This technique measured 100% of remaining particles in each sample to ensure all potential MP particles could be associated to a specific polymer type, or excluded from being classified as plastic. Both extraction and spectroscopic analysis followed protocols to prevent contamination during all steps, including processing blanks to allow estimation of false-positive MP particles that were excluded from final results after interpretation. Contamination from the core tube was not observed.

Persistent organic pollutants and biomarkers. Polycyclic aromatic hydrocarbons (PAHs), dichlorodiphenyltrichloroethane (DDT) and biomarkers (sterols) were analysed at the IOW, Germany (Kaiser and Lerch, 2022; Kanwischer et al., 2020). Briefly, homogenized sediments (0.3–0.8 g dw; $n=62$; Supplemental Table S2) were extracted with a DCM:MeOH mixture using an Accelerated Solvent Extraction device (Dionex™ASE™ 350; Thermo Fisher Scientific). After the addition of internal standards, the extracts were desulfurized with activated copper and separated into four fractions by microscale flash column chromatography using hexane (F1), hexane:DCM (F2), DCM (F3) and DCM:MeOH (F4) as eluting solvents (Kaiser and Arz, 2016). The F1 and derivatized F4 fractions were analysed by gas chromatography - mass spectrometry (GC-MS; Agilent Technologies 7890 B GC system and 5977 B Mass Selective Detector). PAHs, p,p'-DDD (1,1,-dichloro-2,2,-bis(p-chlorophenyl)ethane) and p,p'-DDE (1,1-dichloro-2,2-bis(chlorophenyl)ethylene) were identified by comparing retention time with certified external standards (DRE-L20950009CY and DRE-L18000014CY). PAHs and DDT, considered here as the sum of its two degradation products, p,p'-DDD and p,p'-DDE, were quantified using calibration curves based on six calibrator points and expressed as ΣPAH and ΣDDT . Brassicasterol (24-methylcholesta-5,22E-dien-3 β -ol), tetrahymanol (gammaceran-3 β -ol), coprostanol (5 β -cholestan-3 β -ol), epi-coprostanol, 5 β -stigmastanol (24 β -ethyl-5 β -cholestan-3 β -ol), and epi-5 β -stigmastanol were identified by chromatographic and

mass spectral comparison with published data. The analytical recovery was estimated to 90% and the limit of quantification to 5 ng g^{-1} sediment dw. Results were normalized to the total organic carbon content for each sample ($\mu\text{g gTOC}^{-1}$).

Total carbon (TC), total organic carbon (TOC), total nitrogen (TN), and C/N ratio. Bulk sediment TC, TOC and TN were measured at the IOW, Germany (Müller and Voss, 1999; Voss et al., 2000). The samples (30 mg dw; $n=62$; Supplemental Table S2) were analysed with a Carlo Erba Flash EA elemental analyser. TOC and TN were measured by weighing the sediment into Ag boats and treating it with 2N HCL until all carbonate compounds had reacted out. The sample was dried at 60°C , pelletized and measured. The calibration material for C and N analysis was acetanilide (Merck). The analytical precision was better than 1% for TC and TOC, and better than 4% for TN. The C/N ratio was defined as the molar ratio between TOC and TN: $C/N = (\text{TOC}/12)/(\text{TN}/14)$. Data were not corrected for salt content due to low salinity of the Baltic Sea (Snoeijs-Leijonmalm and André, 2017).

Stable carbon ($\delta^{13}\text{C}$) and nitrogen ($\delta^{15}\text{N}$) isotopes. Bulk $\delta^{15}\text{N}$ and $\delta^{13}\text{C}$ were analysed at the IOW, Germany. Briefly, untreated and treated (acidified) fractions of sediments ($n=62$; Supplemental Table S2) were analysed following Müller and Voss (1999) and Voss et al. (2000). The isotopic compositions were determined using flash combustion in a EA Isolink CN (Thermo Fisher Scientific) elemental analyser at 1020°C coupled via a ConFlo IV (Thermo Fisher Scientific) split interface to a Delta⁺ V advantage (Thermo Fisher Scientific) isotope ratio mass spectrometer. The isotopic values are reported relative to atmospheric N_2 ($\delta^{15}\text{N}$) and Vienna PeeDee Belemnite (VPDB; $\delta^{13}\text{C}$). The reference materials used for stable isotope analysis were IAEA-N1, IAEA-N2, IAEA-N3, NBS 22, IAEA-CH-3 and IAEA-CH-6. The analytical precision for both stable isotope ratios was $<0.2\%$. To correct for the Suess effect, that is a change in $\delta^{13}\text{C}$ by the admixture of large amounts of fossil-fuel derived CO_2 , the following equation (Schelske and Hodell, 1995; Verburg, 2007) was applied:

$$\delta^{13}\text{C}_{\text{org,corr}} = \delta^{13}\text{C}_{\text{org}} - \left(4,577.8 - 7.3430 * y + 3.9213 \times 10^{-3} * y^2 - 6.9812 * 10^{-7} * y^3 \right)$$

where y =year CE.

Inorganic geochemical markers. Sedimentary major and trace element contents and stable Pb isotopes were analysed at the IOW, Germany. Briefly, the sediments (100 mg dw; $n=62$; Supplemental Table S2) were digested with a HNO_3 - HClO_4 -HF mixture in closed Teflon vessels at 180°C for 12 h and the residues were fumed-off 3-times with 6M HCl and finally diluted with 2 vol% HNO_3 (Dellwig et al., 2019). The content of Al was measured by inductively coupled plasma optical emission spectrometry (ICP-OES, iCAP 7400 Duo, Thermo Fisher Scientific) using external calibration and Sc as internal standard. Analytical precision and accuracy were estimated with the international reference material SGR-1b (USGS) and were better than 3.8% and -3.9% , respectively. Trace metals Cu, Pb (including ^{206}Pb and ^{207}Pb) and Zn were determined by inductively coupled plasma mass spectrometry (ICP-MS, iCAP Q, Thermo Fisher Scientific) coupled to a prepFAST system (Elemental Scientific) using He as collision gas, external calibration, and Rh and Ir as internal standards. Analytical precision and accuracy of concentration measurements were also checked with SGR-1b and were better than 3.3% and -3.4% , respectively. For stable Pb isotope ratios, NIST SRM-981 was used resulting in a precision and accuracy of 0.31% and -0.04% ,

respectively (Dellwig et al., 2021). Results were normalized to Al content for each sample to minimize dilution effects caused by organic matter, carbonate and/or opal. To determine Hg contents, sediments (100 mg dw; $n=63$; Supplemental Table S2) were analysed with a Milestone DMA-80 EVO Direct Mercury Analyser by thermal decomposition at 750°C, gold amalgamation and atomic absorption spectrophotometry at 253.65 nm. Data were calibrated against the BCR 142R certified reference material and a Baltic Sea reference sediment. Analytical precision based on reference materials was better than 6%.

Numerical analysis. To detect positions of abrupt change (change-points) within the different datasets, a modelling approach (Gallagher et al., 2011) was applied using the software Past v4.10 (Hammer et al., 2001). Before analysis, the datasets were interpolated every 1 cm, missing values were treated by linear interpolation, and mean and standard deviation were automatically normalized in order to equally weigh each dataset. The default value of 100,000 iterations (Markov chain Monte Carlo) was used and the number of change-point set to $n=1$ (Supplemental Table S3).

Results

Lithology

The lithology of core EMB201/7-4 was characterized by a pronounced visual transition at around 27 cm sediment depth (Figure 2). Between 45 and 27 cm depth the sediment was grey, relatively homogeneous, silty-clay, with low organic carbon and water contents. Between 27 and 0 cm depth it was brown to dark brown and black, cm-thick layered and sometimes laminated, with high organic carbon and water contents. Note that, after oxidation, sediment colours change to dark grey below 27 cm and to brown to dark brown between 27 and 0 cm. The upper part of the core was also characterized by a few light grey, mm-wide, clayey to silty laminations mainly between 21 and 25 cm depth.

Chronology

The use of unsupported ^{210}Pb ($^{210}\text{Pb}_{\text{unsupp}}$) to date recent sediments is challenging in the Baltic Sea because the depositional environment and the sedimentation type have varied over the past 100 years, resulting in an irregular decrease in $^{210}\text{Pb}_{\text{unsupp}}$ (Häusler et al., 2018; Mattila et al., 2006; Moros et al., 2017). Seven parameters were considered to build the stratigraphy ($^{206/207}\text{Pb}$, Hg, ΣPAH , ΣDDT , Mn/Ti, Co/Al and ^{137}Cs ; Figure 2b–h), and twelve stratigraphical events, or time markers, were used to date the sediment (Table 1). The uncertainties of the time markers were estimated following Moros et al. (2017), Kaiser et al. (2018, 2020), and Lin et al. (2021). The early increases in $^{206/207}\text{Pb}$, Hg and ΣPAH reflect the early increase in wood and coal combustion around 1870 CE related to the beginning of the Second Industrial Revolution, or Technological Revolution (Díaz-Somoano et al., 2009; Elmquist et al., 2007; Hanke et al., 2019; Hites et al., 1977). The abrupt rise in ΣDDT is likely related to increased DDT use for agriculture since 1950 CE (Li and Macdonald, 2005), a well-known pattern in Baltic Sea and European lake sediments (Sabatier et al., 2014; Thevenon et al., 2013). Mn and Co enrichments are attributed to four MBIs (1978, 1994, 2003 and 2014 CE; Dellwig et al., 2021; Lin et al., 2021), and tentatively to other four MBIs (1964, 1967, 1970 and 1972 CE; Supplemental Figure S1). The ^{137}Cs increase has been attributed to the Chernobyl accident in 1986 CE. The year of the core recovery (2018 CE) was attributed to the core top layer. Linear sedimentation rates were assumed between time markers

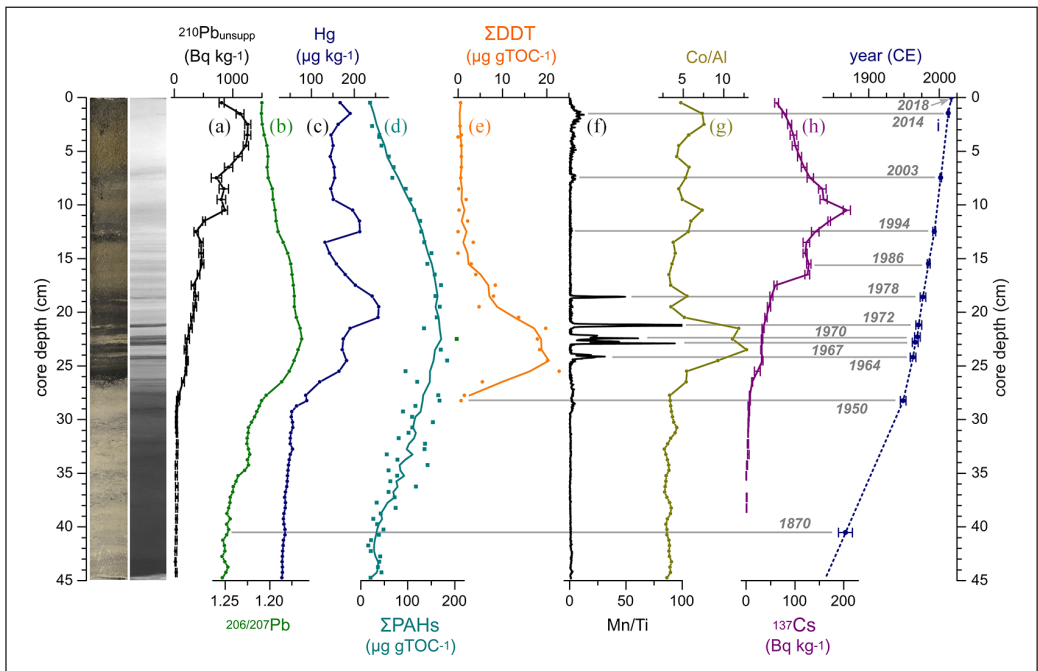


Figure 2. Pictures (true colour and radiography), depth profiles of $^{210}\text{Pb}_{\text{unsupp}}$ (a), $^{206}/^{207}\text{Pb}$ (b), Hg (c), ΣPAH (d) and ΣDDT (e) contents, Mn/Ti (f), Co/Al (g) and ^{137}Cs (h), and age-depth relationship (i) of core EMB201/7-4. The assigned time markers are shown by horizontal grey lines and listed in Table 1.

Table 1. List of the time markers used to establish the age model of core EMB201/7-4.

Sediment depth (cm)	Age (yr CE)	Age error bar (yr)	Marker	Event
0	2018	0.5	Core top	Core recovery
1.5	2014	1	Mn/Ti; Co/Al	Major Baltic Inflow
7.5	2003	1	Mn/Ti; Co/Al	Major Baltic Inflow
12.5	1994	2	Mn/Ti; Co/Al	Major Baltic Inflow
15.5	1986	2	^{137}Cs	Chernobyl accident
18.6	1978	4	Mn/Ti; Co/Al	Major Baltic Inflow
21.2	1972	4	Mn/Ti; Co/Al	Major Baltic Inflow
22.3	1970	4	Mn/Ti; Co/Al	Major Baltic Inflow
22.8	1967	4	Mn/Ti; Co/Al	Major Baltic Inflow
24.2	1964	4	Mn/Ti; Co/Al	Major Baltic Inflow
28.3	1950	4	ΣDDT	Increased DDT usage for agriculture
40.3	1870	10	ΣPAHs ; $^{206}/^{207}\text{Pb}$; Hg	Increasing wood and coal combustion
44.8	1840	10	Core bottom	Extrapolated age

resulting in a mean sedimentation rate increasing from 0.2 cm yr^{-1} between 45 cm (ascribed the date $1840 \pm 10 \text{ CE}$) and 28.4 cm depth ($1950 \pm 4 \text{ CE}$) to 0.4 cm yr^{-1} from 28.4 cm to the top of the core (Figure 2g).

Radioisotopes (actinides and ^{14}C)

^{241}Am and $^{239+240}\text{Pu}$ profiles showed similar patterns (Figure 3a and b). Both radionuclides were close to the detection limit below 28.8 cm depth (1947 ± 4 CE). They started to increase at 27.3 cm depth (1953 ± 4 CE) and reached a maximum at 24.5 cm depth (1963 ± 4 CE) with activities of 8.4 Bq kg^{-1} for ^{241}Am and 0.025 Bq kg^{-1} for $^{239+240}\text{Pu}$. Above this depth, the activities of both radionuclides decreased abruptly. A second, sharp peak occurred at 15.5 cm depth (1986 ± 2 CE) in both radionuclide profiles. Values of $^{240/239}\text{Pu}$ (Figure 3c), a tracer for Pu source, were >0.301 at 28.8 and 28.3 cm depth (1947 ± 4 and 1950 ± 4 CE, respectively) and between 0.160 and 0.219 from 27.8 cm depth (1952 ± 4 CE) except for slightly higher values at 15.5 cm (1986 ± 2 CE) and 10.5 cm depth (1998 ± 2 CE). F^{14}C (Figure 3d), the normalized fraction of ^{14}C (Hajdas et al., 2021), was relatively stable (~ 0.8) between 30.8 and 27.3 cm depth (1933–1953 CE). It started increasing at 26.5 cm depth (1956 ± 4 CE), reached a maximum of 1.2 between 23.5 and 20.5 cm (1966 – 1974 CE), and decreased to 1.0 at 1.5 cm depth (2014 ± 1 CE).

Spheroidal carbonaceous particles. A first appearance of SCPs (Figure 4a) occurred at 36.3 cm depth (1897 ± 8 CE), but SCP contents remained low and sporadic until 27.3 cm depth (1953 ± 4 CE). Only SCPs $<25 \mu\text{m}$ (and frequently $<10 \mu\text{m}$) were observed in this lower section. Above 27.3 cm depth, SCP contents increased, initially rapidly, through to a peak of $>7700 \text{ SCPs g}^{-1} \text{ dw}$ at 16.5 cm depth (1983 ± 3 CE). From this peak, SCP contents showed a general decline through to the top of the core. Above 28.3 cm, larger SCPs appeared for the first time and SCPs had a wide size range from <5 to $>50 \mu\text{m}$ (Supplemental Table S2).

Microplastics. A total of 178 MP particles and six different polymers were identified. Most MP particles were smaller than $100 \mu\text{m}$ in size, and fibres were almost absent. MP amounts (Figure 4b) ranged between 248 and $7135 \text{ MP kg}^{-1} \text{ dw}$. MPs were identified at all depths between 42.3 and 6.5 cm (1857–2005 CE), with a maximum abundance at 20.5 cm depth (1974 ± 4 CE). In terms of polymer diversity, a near-consistent pattern was observed within all layers with predominance of ethylene-propylene-diene monomer rubbers (Supplemental Table S2).

Polycyclic aromatic hydrocarbons and dichlorodiphenyltrichloroethane. The most abundant PAHs were phenanthrene, fluoranthene, pyrene, benzo[a]anthracene, chrysene, benzo[b]fluoranthene, benzo[k]fluoranthene, benzo[a]pyrene, indeno[1,2,3-cd]pyrene, dibenzo[ah]anthracene and benzo[ghi]perylene. Their sum (ΣPAH) increased gradually from 41.3 to 17.5 cm depth (1863–1981 CE), reaching a maximum around $170 \mu\text{g gTOC}^{-1}$, and decreased gradually to reach a minimum of $20 \mu\text{g gTOC}^{-1}$ near the top of the core (Figure 4c). ΣDDT (Figure 4d) was below detection limit between 44.8 and 28.8 cm depth (1840–1947 CE). It increased rapidly at 28.3 cm depth (1950 ± 4 CE) to reach a maximum of $20 \mu\text{g gTOC}^{-1}$ between 25.5 and 21.5 cm depth (1960–1971 CE). After the peak, ΣDDT decreased gradually towards the top of the core to reach contents $<1 \mu\text{g gTOC}^{-1}$.

Total carbon, total organic carbon, total nitrogen, total organic nitrogen, and the C/N ratio. Both TC and TOC values (Figure 5a and b) were relatively constant around 3%–4% between 44.8 and 29.8 cm depth (1840–1940 CE). Above 29.8 cm depth (1940 ± 5 CE), they increased gradually to reach 19.8 and 17.3% at the top of the core, respectively. TC and TOC showed a significant positive linear correlation ($r^2=0.97$). TN values were $<0.5\%$ below 27.8 cm depth (1952 ± 4 CE), followed by a gradual increase to the top of the core, where the values reached 2% (Figure 5c). The C/N ratio (Figure 5d) ranged between 10 and 12 below 27.8 cm depth (1952 ± 4 CE), and between 8 and 10 above 23.5 cm depth (1966 ± 4 CE).

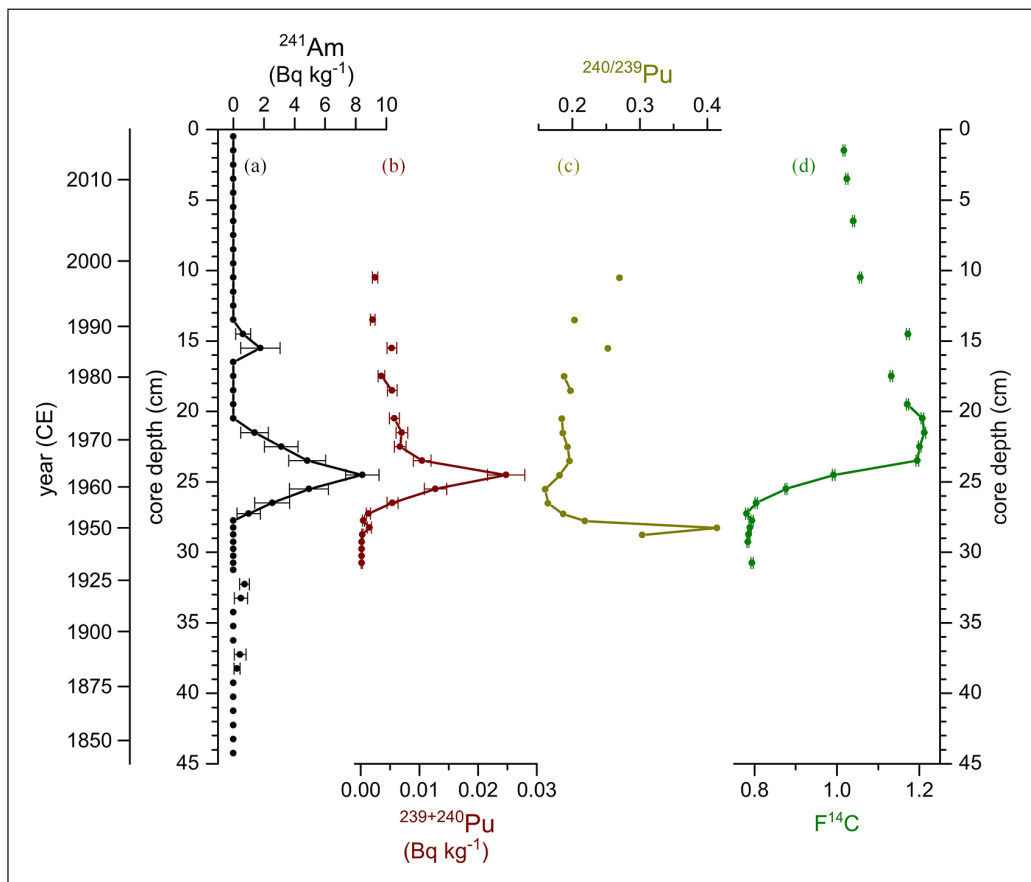


Figure 3. Depth profiles of ^{241}Am (a) and $^{239+240}\text{Pu}$ (b) activities, $^{240/239}\text{Pu}$ (c), and $F^{14}\text{C}$ (d) in core EMB201/7-4.

Stable carbon and nitrogen isotopes. The record of bulk organic matter $\delta^{13}\text{C}$ ($\delta^{13}\text{C}_{\text{org}}$) presented a -1.2‰ shift from $-26.2 \pm 0.2\text{‰}$ below 27.8 cm depth (1952 ± 4 CE) to $-25.0 \pm 0.3\text{‰}$ above this depth (Figure 5e). Both $\delta^{13}\text{C}_{\text{org}}$ and $\delta^{13}\text{C}_{\text{org,corr}}$ vertical profiles (Figure 5e) were relatively similar, except above 11.5 cm depth (1996 ± 2 CE), where $\delta^{13}\text{C}_{\text{org}}$ values decreased gradually compared to $\delta^{13}\text{C}_{\text{org,corr}}$. $\delta^{15}\text{N}$ values presented a relatively large scatter (Figure 5f). A general increasing trend of $+2\text{‰}$ occurred between 44.8 and 27.8 cm depth (1840–1952 CE). Above 26.5 cm depth (1956 ± 4 CE), $\delta^{15}\text{N}$ values fluctuated around $3.3 \pm 0.4\text{‰}$.

Inorganic geochemical signals. Hg/Al , Cu/Al , Zn/Al , and Pb/Al values (Figure 6a–d) increased from 28.8 cm depth (1947 ± 4 CE). The ratios were highest between 24 and 18 cm depth (1966–1978 CE), and decreased until 16.5 cm depth (1983 ± 3 CE). Cu/Al and Zn/Al increased again above 16.5 cm depth (1983 ± 3 CE). $^{206/207}\text{Pb}$ values (Figure 6e) decreased gradually from 1.253 to 1.164 between 38.8–22.5 cm depth (1873–1969 CE) with a slight increase from 33.3 to 31.8 cm depth (1917–1927 CE). Above 22.5 cm depth (1969 ± 4 CE), $^{206/207}\text{Pb}$ values increased and reached a value of 1.209 at the top of the core.

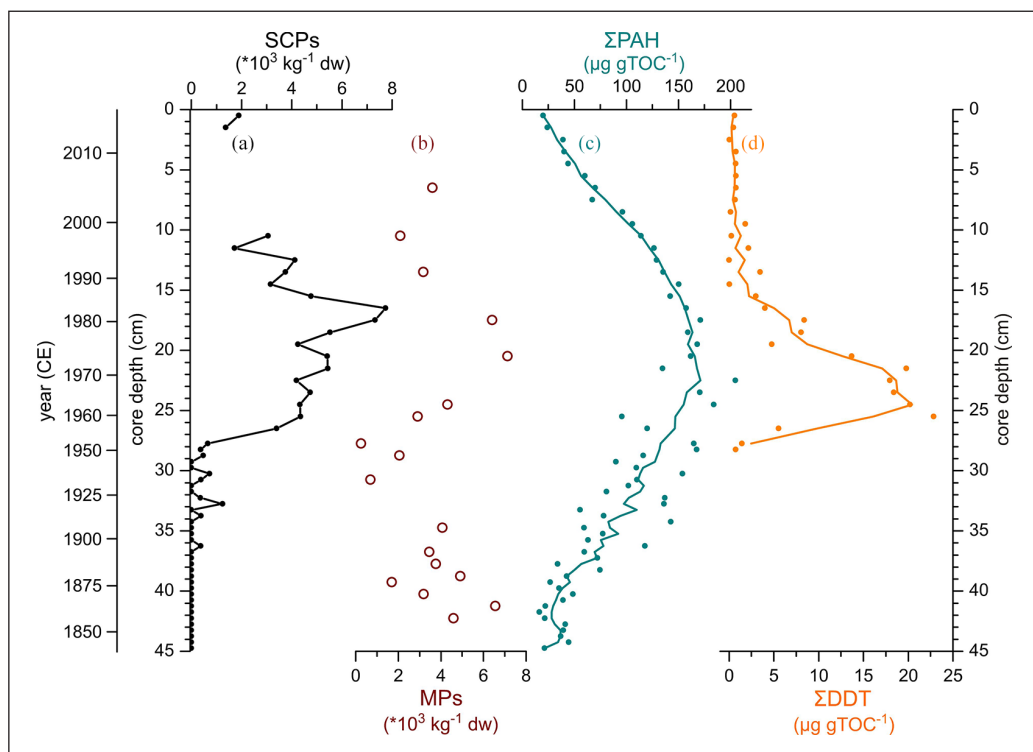


Figure 4. Depth profiles of SCPs (a), microplastics (b), Σ PAH (c) and Σ DDT (d) contents in core EMB201/7-4.

Biotic markers. Brassicasterol, contents increased significantly from 1.5 to 8.5 $\mu\text{g gTOC}^{-1}$ between 26.5 cm depth (1956 \pm 4 CE) and the top of the core (Figure 7a). Tetrahymanol contents (Figure 7b) showed a similar trend with very low values below 26.5 cm depth (1956 \pm 4 CE) followed by an increase until 10.5 cm depth (1998 \pm 2 CE). Above this depth, the contents were relatively stable until the top of the core. Faecal lipids (the sum of coprostanol and epi-coprostanol) first appeared at 26.5 cm depth (1956 \pm 4 CE) and increased until the top of the core (Figure 7c). The R2 ratio (R2 = coprostanol + epicoprostanol / 5 β -stigmastanol + epi-5 β -stigmastanol + coprostanol + epi-coprostanol; Kaiser and Lerch, 2022) ranged between 0.4 and 0.8 and increased from 26.5 cm (1956 \pm 4 CE) to the top of the core (Figure 7d; Supplemental Table S2).

Discussion

Chronology

The age model of core EMB201/7-4 (Figure 2) is well-constrained by eleven stratigraphic events between 1950 and 2018 CE (28.3–0 cm depth). Most of these stratigraphic events are known in the Baltic Sea and have already been used to date recent sediments (Dellwig et al., 2021; Häusler et al., 2018; Kaiser et al., 2020; Lin et al., 2021; Moros et al., 2017). Before 1950 \pm 4 CE (28.3 cm depth), however, the age model is based on a single stratigraphic event at 1870 \pm 10 CE (40.3 cm depth) and on a linear extrapolation to the bottom of the core dated 1840 \pm 10 CE (45 cm depth). Between

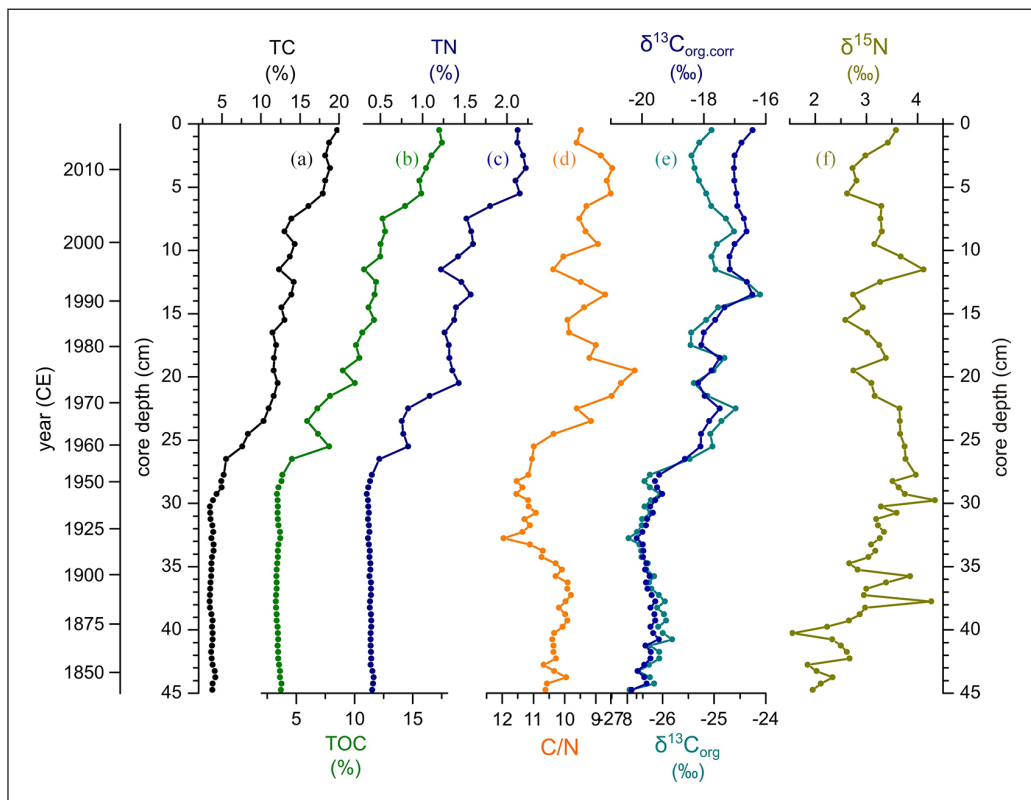


Figure 5. Depth profiles of TC (a), TOC (b), and TN (c) contents, C/N ((d) reversed plotted), $\delta^{13}\text{C}_{\text{org}}$ and $\delta^{13}\text{C}_{\text{org,corr}}$ (e), and $\delta^{15}\text{N}$ (f) in core EMB201/7-4.

1870 and 1950 CE, older-than-expected ^{14}C ages (1892 ± 80 year BP; $n=7$) were obtained (Supplemental Table S2). This indicates an admixture of relatively older organic matter most likely due to the inwash of pre-aged terrestrial organic matter from the drainage basin (Howarth et al., 2013; Schroeter et al., 2021), or sediment reworking (Moros et al., 2020). The $^{206}/^{207}\text{Pb}$ and ΣPAH profiles from core EMB201/7-4 (Figure 2b and d) support the absence of sediment reworking as they are comparable to existing records from lakes within the Baltic Sea drainage basin (Renberg et al., 2001, 2002). Therefore, the inwash of pre-aged terrestrial organic matter likely explains older-than-expected radiocarbon ages, but the sediments were not affected significantly by reworking before 1950 CE. The event stratigraphy approach followed here represents the most advanced method to date Baltic Sea recent sediments.

Radionuclides as primary markers for the Anthropocene GSSP level in Baltic Sea sediments

For the Anthropocene to be a formal chronostratigraphic/geochronologic unit of geological time, a synchronous base is needed (Head et al., 2021; Waters et al., in submission). $^{239+240}\text{Pu}$ and ^{241}Am artificial radionuclides produced by atmospheric nuclear bomb tests are the main candidates as primary markers in the context of the Anthropocene because of their longevity

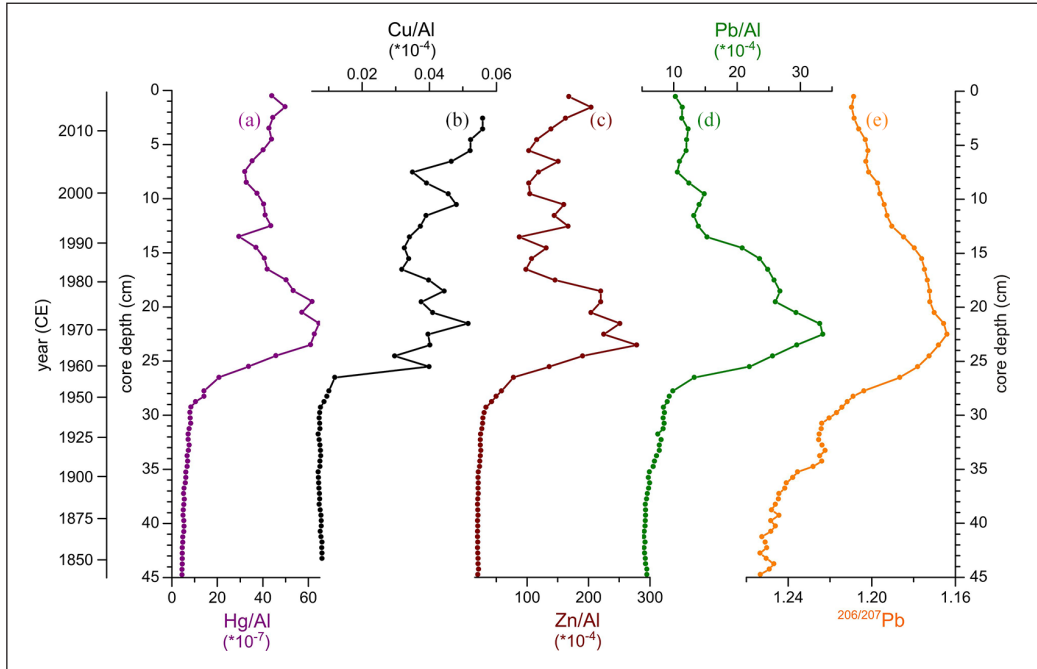


Figure 6. Depth profiles of Hg/Al (a), Cu/Al (b), Zn/Al (c), Pb/Al (d) and $^{206}/^{207}\text{Pb}$ (e) reversed plotted) in core EMB201/7-4.

(half-lives of 24,110 and 432 years, respectively) and appearance around 1950 CE in different archives worldwide (Waters et al., 2018, 2019; Zalasiewicz et al., 2017). While $^{239+240}\text{Pu}$ was first identified above detection limit in 1947 ± 4 CE (28.8 cm depth) in core EMB201/7-4, both ^{241}Am and $^{239+240}\text{Pu}$ (Figure 8a and 8b) started to increase markedly after 1953 ± 4 CE (27.3 cm depth). They reached maximum values in 1963 ± 4 CE (24.5 cm depth), when the Limited Test-Ban Treaty was established, which was followed by a rapid decline in radionuclide fallout worldwide (Waters et al., 2018, 2019). $^{240}/^{239}\text{Pu}$ values (Figure 3c) above 0.30 between 1947 and 1950 CE (28.8–28.3 cm depth) suggested a main radionuclide source from test sites in the Pacific Ocean (Pacific Proving Grounds; Buesseler, 1997; Koide et al., 1985; Lachner et al., 2010; Muramatsu et al., 2000), while values below 0.19 since 1953 ± 4 CE (27.3 cm depth) are typical of global fallout (Buesseler and Sholkovitz, 1987; Kelley et al., 1999). Slightly increased values in 1986 ± 2 CE (15.5 cm depth) are consistent with the Chernobyl accident (Muramatsu et al., 2000).

The ^{137}Cs artificial radionuclide (Figure 2h) activity increased slightly from 1956 ± 4 CE (26.5 cm depth) due to atmospheric nuclear weapon tests, but the most prominent increase occurred after 1981 ± 3 CE (17.5 cm depth) because of the Chernobyl accident in 1986 CE. As documented, the radioactive cloud from this accident first travelled northward and resulted in a high deposition of ^{137}Cs radionuclides in the Baltic Sea region (Dellwig et al., 2018; Ilus et al., 2007; Mattila et al., 2006; Moros et al., 2017). F^{14}C , the atmospheric radiocarbon excess released by nuclear bomb tests, started to increase in 1956 ± 4 CE (26.5 cm depth) and reached maximum values in 1966 ± 4 CE (23.5 cm depth), about three years after ^{241}Am and $^{239+240}\text{Pu}$ in both cases (Figure 3d). This delay can be attributed to atmosphere-ocean ^{14}C equilibration time (Waters et al., 2019).

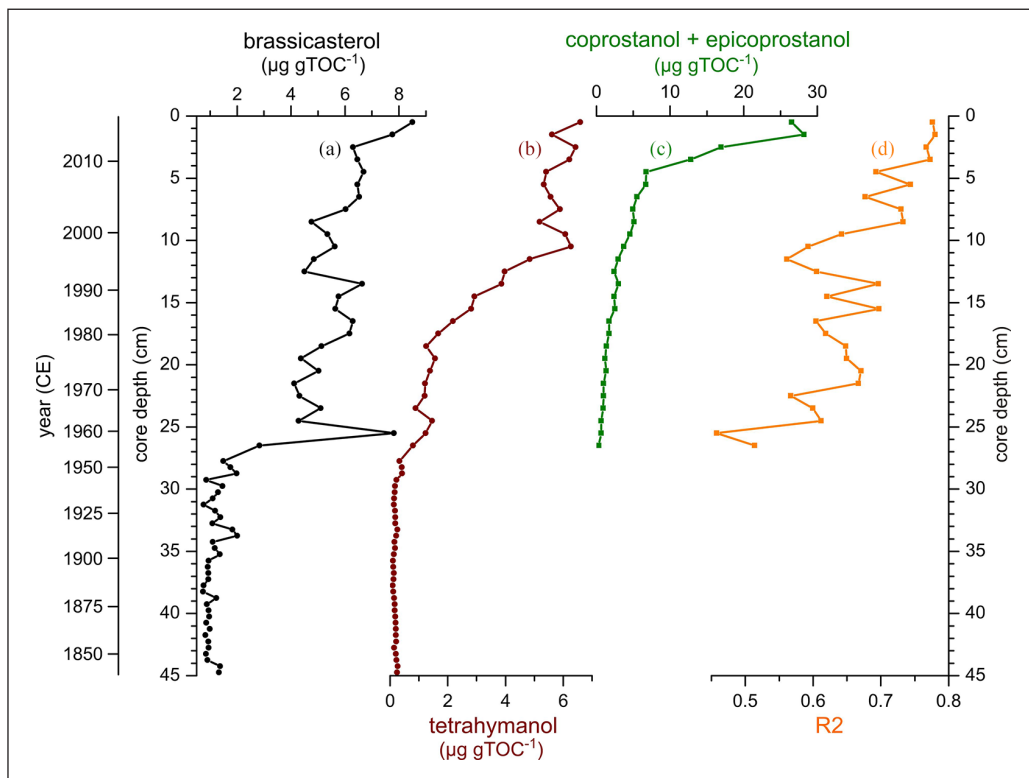


Figure 7. Depth profiles of brassicasterol (a) and tetrahymanol (b) contents, the sum of coprostanol and epicoprostanol contents (c), and the faecal stanol-based R2 ratio (d) in core EMB201/7-4.

Also, post-depositional, vertical migration within sediments, sediment remobilization, as well as sediment inwash from the drainage basin are typical potential issues affecting radionuclide profiles (Davis et al., 1984; Haltia et al., 2021; Hancock et al., 2014; He et al., 1996; Ilus et al., 2007; Mattila et al., 2006; Owens and Walling, 1996; Schroeter et al., 2021; Waters et al., 2019). These issues likely explain the detection of ^{137}Cs since 1917 ± 6 CE (33.3 cm depth) because it is very mobile in sediments compared to ^{241}Am , as well as the detection of radionuclides in the sediments until the present-day.

Artificial $^{239+240}\text{Pu}$ and ^{241}Am radionuclides from nuclear weapons testing are therefore considered here as the most relevant primary markers in the context of the Holocene-Anthropocene boundary. Results from a changepoint model (Figure 8c; Supplemental Table S3) indicated a change starting in 1948 ± 4 CE (28.5 cm depth), but the main change occurred in 1956 ± 4 CE (26.5 cm depth), which would be the proposed GSSP level in Baltic Sea sediments.

Anthropogenic pollutants as secondary markers for the Anthropocene GSSP level in Baltic Sea sediments

SCP contents (Figure 8d) increased markedly after 1953 ± 4 CE (27.3 cm depth) due to an increase in coal and fuel oil combustion related to a high electricity demand after WWII. Furthermore, the introduction of new SCP sources is suggested by their wider range of sizes since that time

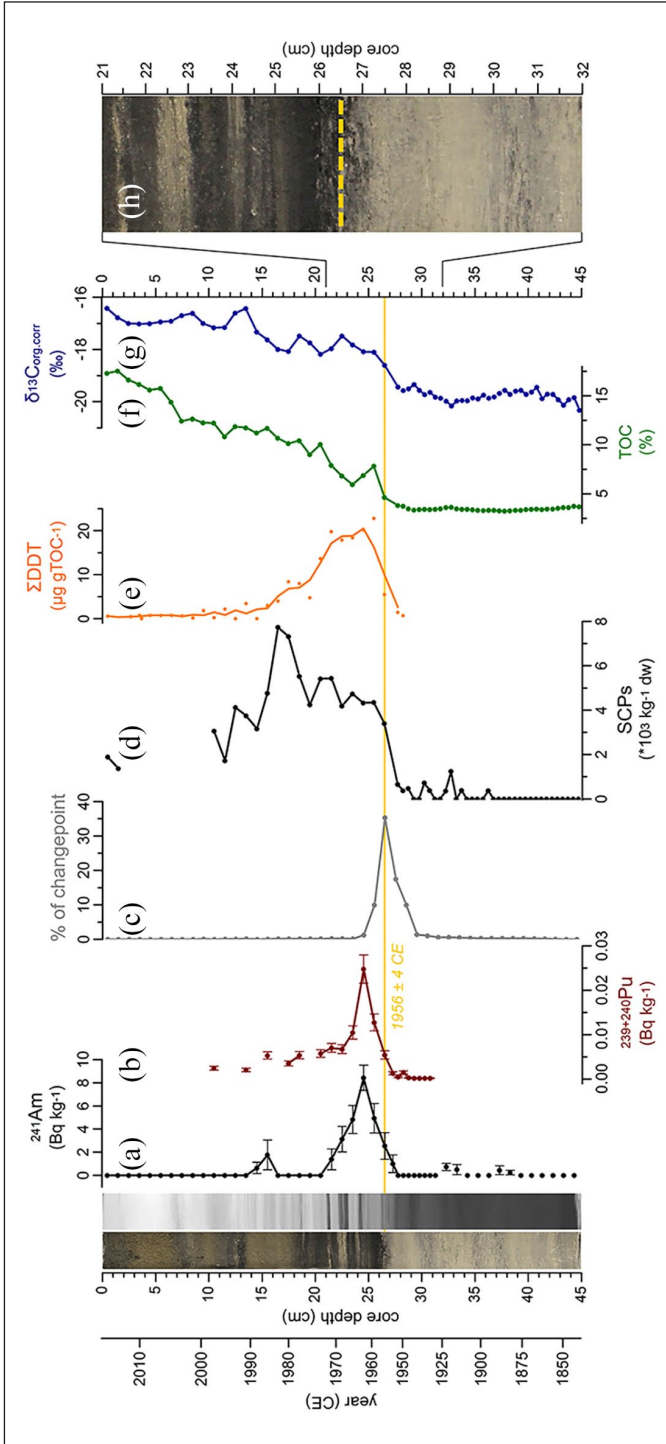


Figure 8. Pictures of core EMB201/7-4 (true colour and radiography), primary markers (a and b), and changepoint modelling results (c) used to define the GSSP level in 1956 ± 4 CE (26.5 cm depth; horizontal line). Secondary markers selected to illustrate changes in anthropogenic pollution (d and e) and eutrophication (f and g) in the Baltic Sea are also shown. A close-up (h) indicating the proposed GSSP level at 26.5 cm in the core is represented by a yellow dotted line.

(Supplemental Table S2). Decreasing SCP contents since 1983 ± 3 CE (16.5 cm depth) reflects the reduction in SCPs release to the atmosphere due to the introduction of particle-arrestor technology since the 1970s and the shift away from coal and oil fuels to natural gas, nuclear and renewable energy sources (Rose, 2015; Rose and Gałuszka, 2019). The Baltic Sea SCP profile is compatible with other lake sediments reported globally (Rose, 2015).

MP amounts (Figure 4b) increased between 1960 and 1974 CE (25.5–20.5 cm depth) as a result of a rapid and intense increase in both production and use of an array of polymer types (Ivar Do Sul and Labrenz, 2020; Zalasiewicz et al., 2016). Ethylene-propylene-diene monomer rubbers, the prevalent category within polymers identified here (Supplemental Table S2), are widely used for a range of marine-and terrestrial-based activities and very common in the marine environment (Lorenz et al., 2019; Primpke et al., 2018). The MP profile suggests that the MP stock in the Baltic Sea marine environment consists of polymers from various provenances affected by different taphonomic processes, and hence does not reflect a direct or straightforward response to world plastic production (Bancone et al., 2020).

Hg, Pb, Cu and Zn are markers of anthropogenic industrial pollution in sediments (Birch et al., 2015; Gałuszka and Rose, 2019; Rauch and Pacyna, 2009). The main trends in Hg/Al, Cu/Al, Zn/Al and Pb/Al (Figure 6a–d) reflect an increase of coal combustion and metal production after the mid-20th century, and a decrease from 1970s CE due to a reduction in industrial dust emission and fossil fuel combustion in northern and western Europe (Callender, 2014; Gałuszka and Wagreich, 2019; Rühling and Tyler, 2001). However, a decrease to background levels in present-day sediments is not observed for most of the metals. This is because trace metals are generally sensitive to changing redox conditions (Bruland et al., 2013), which biases the anthropogenic signal in Baltic Sea sediments. $^{206/207}\text{Pb}$ is not redox-sensitive, and reflects therefore an unbiased signal (Figure 6e). Decreasing $^{206/207}\text{Pb}$ values between the early-1870s CE and the late-1960s CE are most likely due to both increasing coal combustion during the Second Industrial Revolution and the spread of leaded gasoline combustion in Europe since 1950 CE (Boyle et al., 2014; Díaz-Somoano et al., 2009; Renberg et al., 2002). Increasing values since the early-1970s (21.5 cm depth) reflect the decline of lead pollution in Europe due to both the implementation of stricter industrial emission standards and the phase-out of alkyl-lead gasoline (Renberg et al., 2001, 2002).

The appearance of the persistent organic pollutant DDT (Figure 8e) in 1950 ± 4 CE (28.3 cm depth) and its pronounced increase up to 1960 ± 4 CE (25.5 cm depth) is related to the increasing use of DDT in Baltic Sea countries after 1945 CE to control insects on agricultural crops. Indeed, the former Soviet Union had the second highest (after the United States) historical DDT usage in agriculture from 1952 to 1971 CE (Li and Macdonald, 2005). The decrease in DDT content after 1971 ± 4 CE (21.5 cm depth) reflects the ban on its use within Baltic Sea countries since the early-1970s (HELCOM, 2010).

Coprostanol and epicoprostanol faecal lipids (Figure 7c and d) first appeared in 1956 ± 4 CE (26.5 cm depth) and increased subsequently as a result of increasing sewage pollution in the central Baltic Sea (Kaiser and Lerch, 2022). The fraction of human-derived faecal lipids was also increasing since 1956 ± 4 CE as suggested by higher R2 values. Therefore, sedimentary faecal lipids reflect the increasing human-derived sewage pollution related to population growth in the Baltic Sea drainage basin (Kaiser and Lerch, 2022).

For anthropogenic pollutants, results from the changepoint model (Supplemental Table S3) indicated a change starting in 1956 ± 4 CE (26.5 cm depth). This change is, however, more pronounced in 1960 ± 4 CE (25.5 cm depth), which corresponds closely to the inflection point of many indicators of the Great Acceleration (Head et al., 2021).

Organic proxies as secondary markers for the Anthropocene GSSP level in Baltic Sea sediments

The pronounced increase in TOC values (Figure 8f) since 1956 ± 4 CE (26.5 cm depth) reflects the growing burial of phytoplankton biomass under hypoxic conditions due to the eutrophication of the central Baltic Sea deep basins since 1950 CE (Emeis et al., 2000; Struck et al., 2000). Indeed, a shift towards heavier $\delta^{13}\text{C}_{\text{org,corr}}$ values (Figure 8g) after 1952 ± 4 CE (27.8 cm depth) indicates a higher proportion of phytoplankton biomass, as organisms are forced to use the heavier C isotope (^{13}C) when primary production is high (Mizutani and Wada, 1982; Struck et al., 2000; Teranes and Bernasconi, 2005). A decrease in C/N values (Figure 5e) after 1960 ± 4 CE (25.5 cm depth) also indicates an increasing fraction of phytoplankton biomass in Baltic Sea sediments (Emeis et al., 2000; Lamb et al., 2006). The contents of brassicasterol (Figure 7a), or ‘diatomsterol’, a biomarker for the occurrence of diatoms, increased substantially after 1952 ± 4 CE (27.8 cm depth), also indicating the growth of phytoplankton biomass mainly due to eutrophication. The similar increase in tetrahymanol contents (Figure 7b) reflects the concomitant development of a pelagic redoxcline in the central Baltic Sea as tetrahymanol is a biomarker for ciliates thriving abundantly near the redoxclines of hypoxic environments (Anderson et al., 2012; Edgcomb and Pachiadaki, 2014; Harvey and Mcmanus, 1991; Pachiadaki et al., 2014).

An increasing trend in $\delta^{15}\text{N}$ values (Figure 5f) between 1840 and 1950 CE (44.8–28.3 cm depth) resulted most likely from the phytoplankton assimilation of land-derived, isotopically heavier nitrate inputs (Renberg et al., 2001; Struck et al., 2000). Indeed, large-scale changes in land use occurred in the Baltic Sea watershed after the beginning of the Second Industrial Revolution (Zillén and Conley, 2010). After 1950 CE, however, $\delta^{15}\text{N}$ values started to decrease slightly, possibly due to higher inputs of isotopically lighter nitrogen, and increasing biomass of diazotrophic cyanobacteria, an important contributor to the pelagic N-cycle of the central Baltic Sea since 1950 CE (Kaiser et al., 2020; Kendall et al., 2007; Struck et al., 1998, 2000; Voß et al., 1997). Periods with increasing $\delta^{15}\text{N}$ values after 1950 CE may be related to higher inputs of isotopically heavier, wastewater to the Baltic Sea (Kendall et al., 2007).

As shown for anthropogenic pollution markers, the results from the changepoint model (Supplemental Table S3) suggested that the main change in organic proxies occurred in 1960 ± 4 CE (25.5 cm depth), synchronously with many indicators of the Great Acceleration (Head et al., 2021; Syvitski et al., 2020).

Final remarks regarding the Baltic Sea as GSSP for the Anthropocene series

The present study supports the Anthropocene as a stratigraphically substantiated unit, that should be defined by a GSSP and formalized at the rank of epoch with an inception at around 1950 CE (Zalasiewicz et al., 2017). Artificial radioisotopes released during atmospheric nuclear weapons testing, which are the most significant markers in the context the Anthropocene, showed a main change in core EMB201/7-4 in 1956 ± 4 CE as indicated by the changepoint model. This point is therefore proposed as the GSSP level for the Anthropocene series (Figure 8). It corresponds to a marked change in lithology and sediment colour from light grey to dark brown (or dark grey to brown after oxidation), which reflects the beginning of eutrophication in the central Baltic Sea due to an increasing anthropogenic pressure. Despite the most accurate approach used to date core EMB201/7-4, the lack of annual lamination may flag the Baltic Sea as a GSSP candidate for the Anthropocene series.

If accepted, the East Gotland Basin GSSP would be in accordance to all 65 GSSPs presently ratified, which occur within strata deposited in marine sedimentary environments with the

exception of the three Holocene GSSPs (Walker et al., 2018; Waters et al., 2019). The archived half of core EMB201/7-4 is preserved and accessible at the IOW, Germany. Although marine GSSP sites are not as accessible as terrestrial ones, new sediment cores from exactly the same location can be recovered during expeditions on board research vessels. Finally, if appropriate, the name ‘Baltician’ is suggested as potential stage/age (Luciano, 2022).

Acknowledgements

We are thankful to Nadine Hollman, Anne Köhler, Iris Liskow and Ines Scherff for analytical assistance and to the crew and captain of R/V Elisabeth Mann Borgese during expedition EMB201. We also thank the associate editor C.W. and two anonymous reviewers for their valuable comments and suggestions, which improved quality of this manuscript. Analysis of the EMB201/7-4 core was facilitated by the collaborative research project between the Leibniz Institute for Baltic Sea Research (IOW) and the Anthropocene Working Group (AWG) to ratify the stratigraphic Anthropocene. The AWG is co-ordinating the assessment of candidate GSSP sites in collaboration with the Haus der Kulturen der Welt (HKW, Berlin) in the framework of its long-term project Anthropocene Curriculum. The Anthropocene Curriculum is an international project for experimental forms of Anthropocene research and education developed by HKW and the Max Planck Institute for the History of Science (MPIWG, Berlin) since 2013. JA Ivar do Sul is supported by the LABPLAS Project (LAnd-Based Solutions for PLAStics in the Sea, Grant Agreement Nr.: 101003954), financed by the EU Horizon 2020 programme.

Declaration of conflicting interests

The author(s) declared no potential conflicts of interest with respect to the research, authorship, and/or publication of this article.


Funding

The author(s) disclosed receipt of the following financial support for the research, authorship, and/or publication of this article: This work was supported by the Haus der Kulturen der Welt (HKW, Berlin, Germany).

ORCID iDs

Jérôme Kaiser  <https://orcid.org/0000-0002-0290-9088>

Irka Hajdas  <https://orcid.org/0000-0003-2373-2725>

Juliana A Ivar do Sul  <https://orcid.org/0000-0003-0851-3559>

Supplemental material

Supplemental material for this article is available online.

References

- Abel SM, Primpke S, Int-Veen I, et al. (2021) Systematic identification of microplastics in abyssal and hadal sediments of the Kuril Kamchatka trench. *Environmental Pollution* 269: 116095.
- Andersen JH, Carstensen J, Conley DJ, et al. (2017) Long-term temporal and spatial trends in eutrophication status of the Baltic Sea. *Biological Reviews of the Cambridge Philosophical Society* 92: 135–149.
- Anderson R, Winter C and Jürgens K (2012) Protist grazing and viral lysis as prokaryotic mortality factors at Baltic Sea oxic–anoxic interfaces. *Marine Ecology Progress Series* 467: 1–14.
- Bancone CE, Turner SD and Ivar Do Sul JA (2020) The paleoecology of microplastic contamination. *Frontiers in Environmental Science* 8: 574008.
- Birch G, Gunns T and Olmos M (2015) Sediment-bound metals as indicators of anthropogenic change in estuarine environments. *Marine Pollution Bulletin* 101: 243–257.

- Boyle EA, Lee J-M, Echegoyen Y, et al. (2014) Anthropogenic lead emissions in the ocean: The evolving global experiment. *Oceanography* 27: 69–75.
- Brenner WW (2001) Organic-walled microfossils from the central Baltic Sea, indicators of environmental change and base for ecostratigraphic correlation. *Baltica* 14: 40–51.
- Bruland KW, Middag R and Lohan MC (2013) Controls of trace metals in seawater. In: Mottl MJ and Elderfield H (eds) *Treatise on Geochemistry*, 2nd edition. Philadelphia, USA: Saunders, Elsevier Inc., pp.19–51.
- Buesseler KO (1997) The isotopic signature of fallout plutonium in the North Pacific. *Journal of Environmental Radioactivity* 36: 69–83.
- Buesseler KO and Sholkovitz ER (1987) The geochemistry of fallout plutonium in the North Atlantic: II. $^{240}\text{Pu}/^{239}\text{Pu}$ ratios and their significance. *Geochimica et Cosmochimica Acta* 51: 2623–2637.
- Callender E (2014) 11.3 - Heavy metals in the environment – historical trends. In: Holland HD and Turekian KK (eds) *Treatise on Geochemistry*, 2nd edition. Oxford: Elsevier, pp.59–89.
- Carstensen J, Andersen JH, Gustafsson BG, et al. (2014) Deoxygenation of the Baltic Sea during the last century. *Proceedings of the National Academy of Sciences* 111: 5628–5633.
- Davis RB, Hess CT, Norton SA, et al. (1984) ^{137}Cs and ^{210}Pb dating of sediments from soft-water lakes in New England (U.S.A.) and Scandinavia, a failure of ^{137}Cs dating. *Chemical Geology* 44: 151–185.
- Dellwig O, Schnetger B, Meyer D, et al. (2018) Impact of the major Baltic inflow in 2014 on manganese cycling in the Gotland Deep. *Frontiers in Marine Science* 5: 248.
- Dellwig O, Wegwerth A and Arz HW (2021) Anatomy of the major Baltic inflow in 2014: Impact of manganese and iron shuttling on phosphorus and trace metals in the Gotland Basin, Baltic Sea. *Continental Shelf Research* 223: 104449.
- Dellwig O, Wegwerth A, Schnetger B, et al. (2019) Dissimilar behaviors of the geochemical twins W and Mo in hypoxic-euxinic marine basins. *Earth-Science Reviews* 193: 1–23.
- Díaz-Somoano M, Me K, López-Antón MA, et al. (2009) Stable lead isotope compositions in selected coals from around the world and implications for present day aerosol source tracing. *Environmental Science Technology* 43: 1078–1085.
- Edgcomb VP and Pachiadaki M (2014) Ciliates along oxyclines of permanently stratified marine water columns. *Journal of Eukaryotic Microbiology* 61: 434–445.
- Elken J and Matthäus W (2008) *Baltic Sea Oceanography*. In: The BACC Author Team (Ed.), Assessment of Climate Change for the Baltic Sea Basin. Berlin: Springer Verlag, pp. 379–385.
- Elmqvist M, Zencak Z and Gustafsson Ö (2007) A 700 year sediment record of black carbon and polycyclic aromatic hydrocarbons near the EMEP air monitoring station in aspveten, Sweden. *Environmental Science & Technology* 41: 6926–6932.
- Emeis K-C, Struck U, Leipe T, et al. (2000) Changes in the C, N, P burial rates in some Baltic Sea sediments over the last 150 years—relevance to P regeneration rates and the phosphorus cycle. *Marine Geology* 167: 43–59.
- Enders K, Lenz R, Ivar Do, Sul JA, et al. (2020) When every particle matters: A QuEChERS approach to extract microplastics from environmental samples. *MethodsX* 7: 100784.
- Gallagher K, Bodin T, Sambridge M, et al. (2011) Inference of abrupt changes in noisy geochemical records using transdimensional changepoint models. *Earth and Planetary Science Letters* 311: 182–194.
- Gałuszka A and Rose N (2019) Organic compounds. In: Zalasiewicz J, Waters C, Williams M, et al. (eds) *The Anthropocene as a Geological Time Unit: A Guide to the Scientific Evidence and Current Debate*. Cambridge: Cambridge University Press, pp.186–192.
- Gałuszka A and Wagreich M (2019) Metals. In: Zalasiewicz J, Williams M, Waters C, et al. (eds) *The Anthropocene as a Geological Time Unit*. Cambridge: Cambridge University Press, pp.178–186.
- Gustafsson BG, Schenk F, Blenckner T, et al. (2012) Reconstructing the development of Baltic sea eutrophication 1850–2006. *Ambio* 41: 534–548.
- Hajdas I (2008) Radiocarbon dating and its applications in Quaternary studies. *E&G Quaternary Science Journal* 57: 2–24.
- Hajdas I, Ascough P, Garnett MH, et al. (2021) Radiocarbon dating. *Nature Reviews Methods Primers* 1: 62.
- Håkanson L, Lundin L-C, Savchuk O, et al. (2003) The Baltic Sea. In: Rydén L, Migula P and Andersson M (eds) *Environmental Science*. Uppsala: The Baltic University Press, pp.120–146.

- Haltia E, Leppänen A-P, Kallio A, et al. (2021) Sediment profile dating and reconstructing nuclear events from annually laminated lake sediments in northern Finland. *Journal of Environmental Radioactivity* 233: 106611.
- Hammer O, David ATH and Ryan PD (2001) PAST: Paleontological Statistics Software Package for Education and data analysis. *Palaeontologia Electronica* 4: 1–9.
- Hancock GJ, Wilkinson SN, Hawdon AA, et al. (2014) Use of fallout tracers ⁷Be, ²¹⁰Pb and ¹³⁷Cs to distinguish the form of sub-surface soil erosion delivering sediment to rivers in large catchments. *Hydrological Processes* 28: 3855–3874.
- Hanke UM, Lima-Braun AL, Eglinton TI, et al. (2019) Significance of perylene for source allocation of terigenous organic matter in aquatic sediments. *Environmental Science & Technology* 53: 8244–8251.
- Harvey HR and Mcmanus GB (1991) Marine ciliates as a widespread source of tetrahymanol and hopan-3 β -ol in sediments. *Geochimica et Cosmochimica Acta* 55: 3387–3390.
- Häusler K, Dellwig O, Schmetger B, et al. (2018) Massive Mn carbonate formation in the Landsort Deep (Baltic Sea): Hydrographic conditions, temporal succession, and Mn budget calculations. *Marine Geology* 395: 260–270.
- Head MJ, Steffen W, Fagerlind D, et al. (2021) The Great Acceleration is real and provides a quantitative basis for the proposed Anthropocene Series/Epoch. *Eposides*. Epub ahead of print 15 November 2021.
- HELCOM (2010) *Ecosystem health of the Baltic Sea 2003–2007. HELCOM Initial Holistic Assessment, Balt. Sea Environ. Proc. No. 122*. Helsinki: Helsinki Commission.
- He Q, Walling DE and Owens PN (1996) Interpreting the ¹³⁷Cs profiles observed in several small lakes and reservoirs in southern England. *Chemical Geology* 129: 115–131.
- Hites RA, Laflamme RE and Farrington JW (1977) Sedimentary polycyclic aromatic hydrocarbons: The historical record. *Science* 198: 829–831.
- Howarth JD, Fitzsimons SJ, Jacobsen GE, et al. (2013) Identifying a reliable target fraction for radiocarbon dating sedimentary records from lakes. *Quaternary Geochronology* 17: 68–80.
- Ilus E, Mattila J, Nielsen SP, et al. (2007) *Long-lived radionuclides in the seabed of the Baltic Sea*. Report of the Sediment Baseline Study of HELCOM MORS-PRO in 2000–2005, Baltic Sea Environment Proceedings No. 110. Helsinki, Finland: Helsinki Commission Baltic Marine Environment Protection Commission.
- Ivar Do Sul JA and Labrenz M (2020) Microplastics into the Anthropocene: rise and fall of the human footprint. In: Rocha-Santos T, Costa MF and Mouneyrac C (eds) *Handbook of Microplastics in the Environment*. Cham: Springer, pp.1–16.
- Kaiser J and Arz HW (2016) Sources of sedimentary biomarkers and proxies with potential paleoenvironmental significance for the Baltic Sea. *Continental Shelf Research* 122: 102–119.
- Kaiser J and Lerch M (2022) Sedimentary faecal lipids as indicators of Baltic Sea sewage pollution and population growth since 1860 AD. *Environmental Research* 204: 112305.
- Kaiser J, Moros M, Tomczak M, et al. (2018) The invasive diatom *Pseudosolenia calcaravis* and specific C25 isoprenoid lipids as a sedimentary time marker in the Black Sea. *Geology* 46: 507–510.
- Kaiser J, Wasmund N, Kahru M, et al. (2020) Reconstructing N₂-fixing cyanobacterial blooms in the Baltic Sea beyond observations using 6- and 7-methylheptadecane in sediments as specific biomarkers. *Biogeosciences* 17: 2579–2591.
- Kanwischer M, Bunke D, Leipe T, et al. (2020) Polycyclic aromatic hydrocarbons in the Baltic Sea - pre-industrial and industrial developments as well as current status. *Marine Pollution Bulletin* 160: 111526.
- Kelley JM, Bond LA and Beasley TM (1999) Global distribution of Pu isotopes and ²³⁷Np. *The Science of the Total Environment* 237–238: 483–500.
- Kendall C, Elliott EM and Wankel SD (2007) Tracing anthropogenic inputs of nitrogen to ecosystems. *Stable isotopes in ecology and environmental science* 2: 375–449.
- Koide M, Bertine KK, Chow TJ, et al. (1985) The ²⁴⁰Pu/²³⁹Pu ratio, a potential geochronometer. *Earth and Planetary Science Letters* 72: 1–8.
- Lachner J, Christl M, Bisinger T, et al. (2010) Isotopic signature of plutonium at Bikini atoll. *Applied Radiation and Isotopes* 68: 979–983.
- Lamb AL, Wilson GP and Leng MJ (2006) A review of coastal palaeoclimate and relative sea-level reconstructions using $\delta^{13}\text{C}$ and C/N ratios in organic material. *Earth-Science Reviews* 75: 29–57.

- Lepland A and Stevens RL (1998) Manganese authigenesis in the Landsort Deep, Baltic Sea. *Marine Geology* 151: 1–25.
- Lin M, Qiao J, Hou X, et al. (2021) 70-Year anthropogenic uranium imprints of nuclear activities in Baltic Sea sediments. *Environmental Science & Technology* 55: 8918–8927.
- Li Y-F and Macdonald RW (2005) Sources and pathways of selected organochlorine pesticides to the Arctic and the effect of pathway divergence on HCH Trends in Biota: A review. *The Science of the Total Environment* 342: 87–106.
- Lokas E, Wachniew P, Baccolo G, et al. (2022) Unveiling the extreme environmental radioactivity of cryocoinite from a Norwegian glacier. *The Science of the Total Environment* 814: 152656.
- Lorenz C, Roscher L, Meyer MS, et al. (2019) Spatial distribution of microplastics in sediments and surface waters of the southern North Sea. *Environmental Pollution* 252: 1719–1729.
- Luciano E (2022) Is ‘Anthropocene’ a suitable chronostratigraphic term? *Anthropocene Science* 1: 29–41.
- Mattila J, Kankaanpää H and Ilus E (2006) Estimation of recent sediment accumulation rates in the Baltic Sea using artificial radionuclides ¹³⁷Cs and ^{239,240}Pu as time markers. *Boreal Environment Research* 11: 95–107.
- Mizutani H and Wada E (1982) Effect of high atmospheric CO₂ concentration on δ^{13} of algae. *Origins of Life* 12: 377–390.
- Mohrholz V (2018) Major Baltic inflow statistics – Revised. *Frontiers in Marine Science* 5: 384.
- Mohrholz V, Naumann M, Nausch G, et al. (2015) Fresh oxygen for the Baltic Sea — An exceptional saline inflow after a decade of stagnation. *Journal of Marine Systems* 148: 152–166.
- Moros M, Andersen TJ, Schulz-Bull D, et al. (2017) Towards an event stratigraphy for Baltic Sea sediments deposited since AD 1900: Approaches and challenges. *Boreas* 46: 129–142.
- Moros M, Kotilainen AT, Snowball I, et al. (2020) Is ‘deep-water formation’ in the Baltic Sea a key to understanding seabed dynamics and ventilation changes over the past 7,000 years? *Quaternary International* 550: 55–65.
- Müller A and Voss M (1999) The palaeoenvironments of coastal lagoons in the southern Baltic Sea, II. δ^{13} C and δ^{15} N ratios of organic matter — Sources and sediments. *Palaeogeography Palaeoclimatology Palaeoecology* 145: 17–32.
- Muramatsu Y, Rühm W, Yoshida S, et al. (2000) Concentrations of ²³⁹Pu and ²⁴⁰Pu and their isotopic ratios determined by ICP-MS in soils collected from the Chernobyl 30-km zone. *Environmental Science & Technology* 34: 2913–2917.
- Němec M, Wacker L, Hajdas I, et al. (2010) Alternative methods for cellulose preparation for AMS measurement. *Radiocarbon* 52: 1358–1370.
- OSPAR. 1998. Principles of the Comprehensive Study on Riverine Inputs and Direct Discharges (RID). 1998-5, London: OSPAR Commission.
- Owens PN and Walling DE (1996) Spatial variability of caesium-137 inventories at reference sites: An example from two contrasting sites in England and Zimbabwe. *Applied Radiation and Isotopes* 47: 699–707.
- Pachiadaki MG, Yakimov MM, LaCono V, et al. (2014) Unveiling microbial activities along the halocline of Thetis, a deep-sea hypersaline anoxic basin. *The ISME Journal* 8: 2478–2489.
- Passow, U. 1991. Species-specific sedimentation and sinking velocities of diatoms. *Marine Biology* 108: 449–455.
- Primpke S, Wirth M, Lorenz C, et al. (2018) Reference database design for the automated analysis of microplastic samples based on Fourier transform infrared (FTIR) spectroscopy. *Analytical and Bioanalytical Chemistry* 410: 5131–5141.
- Rauch JN and Pacyna JM (2009) Earth’s global Ag, Al, Cr, Cu, Fe, Ni, Pb, and Zn cycles. *Global Biogeochemical Cycles* 23: GB2001.
- Reimer PJ, Brown TA and Reimer RW (2004) Discussion: Reporting and calibration of post-bomb ¹⁴C data. *Radiocarbon* 46: 1299–1304.
- Renberg I, Bindler R and Brännvall M-L (2001) Using the historical atmospheric lead-deposition record as a chronological marker in sediment deposits in Europe. *The Holocene* 11: 511–516.

- Renberg I, Brännvall ML, Bindler R, et al. (2002) Stable lead isotopes and lake sediments—a useful combination for the study of atmospheric lead pollution history. *The Science of the Total Environment* 292: 45–54.
- Reusch TBH, Dierking J, Andersson HC, et al. (2018) The Baltic Sea as a time machine for the future coastal ocean. *Science Advances* 4: eaar8195.
- Rose NL and Gałuszka A (2019) Novel materials as particulates. In: Zalasiewicz J, Waters C and Williams M (eds) *The Anthropocene as a Geological Time Unit: A Guide to the Scientific Evidence and Current Debate*. Cambridge: Cambridge University Press, pp.51–58.
- Rose NL (1994) A note on further refinements to a procedure for the extraction of carbonaceous fly-ash particles from sediments. *Journal of Paleolimnology* 11: 201–204.
- Rose NL (2008) Quality control in the analysis of lake sediments for spheroidal carbonaceous particles. *Limnology and Oceanography Methods* 6: 172–179.
- Rose NL (2015) Spheroidal carbonaceous fly ash particles provide a globally synchronous stratigraphic marker for the Anthropocene. *Environmental Science & Technology* 49: 4155–4162.
- Rühling and Tyler G (2001) Changes in atmospheric deposition rates of heavy metals in Sweden a summary of nationwide Swedish surveys in 1968/70–1995. *Water Air and Soil Pollution Focus* 1: 311–323.
- Sabatier P, Poulenard J, Fanget B, et al. (2014) Long-term relationships among pesticide applications, mobility, and soil erosion in a vineyard watershed. *Proceedings of the National Academy of Sciences* 111: 15647–15652.
- Schelske CL and Hodell DA (1995) Using carbon isotopes of bulk sedimentary organic matter to reconstruct the history of nutrient loading and eutrophication in Lake Erie. *Limnology and Oceanography* 40: 918–929.
- Schroeter N, Mingram J, Kalanke J, et al. (2021) The reservoir age effect varies with the mobilization of pre-aged organic carbon in a high-altitude Central Asian catchment. *Earth Science Frontiers* 9: 532.
- Snoeijs-Leijonmalm P and Andrén E (2017) Why is the Baltic Sea so special to live in? In: Snoeijs-Leijonmalm P, Schubert H and Radziejewska T (eds) *Biological Oceanography of the Baltic Sea*. Dordrecht: Springer Netherlands, pp.23–84.
- Sohlenius G and Westman P (1998) Salinity and redox alternations in the northwestern Baltic proper during the late holocene. *Boreas* 27: 101–114.
- Struck U, Emeis K-C, Voss M, et al. (2000) Records of southern and central Baltic Sea eutrophication in $\delta^{13}\text{C}$ and $\delta^{15}\text{N}$ of sedimentary organic matter. *Marine Geology* 164: 157–171.
- Struck U, Emeis K-C, Voß M, et al. (2001) Biological productivity during sapropel S5 formation in the Eastern Mediterranean Sea: Evidence from stable isotopes of nitrogen and carbon. *Geochimica et Cosmochimica Acta* 65: 3249–3266.
- Struck U, Voss M, von Bodungen B, et al. (1998) Stable isotopes of nitrogen in fossil cladoceran exoskeletons: Implications for nitrogen sources in the central Baltic Sea during the past century. *Die Naturwissenschaften* 85: 597–603.
- Stuiver M and Polach HA (1977) Reporting of C-14 data-Discussion. *Radiocarbon* 19: 355–363.
- Synal H-A, Jacob S and Suter M (2000) The PSI/ETH small radiocarbon dating system. *Nuclear Instruments & Methods in Physics Research Section B, Beam Interactions With Materials and Atoms* 172: 1–7.
- Syvitski J, Waters CN, Day J, et al. (2020) Extraordinary human energy consumption and resultant geological impacts beginning around 1950 CE initiated the proposed Anthropocene Epoch. *Communications Earth & Environment* 1: 32.
- Teranes JL and Bernasconi SM (2005) Factors controlling $\delta^{13}\text{C}$ values of sedimentary carbon in hypertrophic Baldeggersee, Switzerland, and implications for interpreting isotope excursions in lake sedimentary records. *Limnology and Oceanography* 50: 914–922.
- Thevenon F, Alencastro LFD, Loizeau J-L, et al. (2013) A high-resolution historical sediment record of nutrients, trace elements and organochlorines (DDT and PCB) deposition in a drinking water reservoir (Lake Brêt, Switzerland) points at local and regional pollutant sources. *Chemosphere* 90: 2444–2452.
- Verburg P (2007) The need to correct for the Suess effect in the application of $\delta^{13}\text{C}$ in sediment of autotrophic Lake Tanganyika, as a productivity proxy in the Anthropocene. *Journal of Paleolimnology* 37: 591–602.

- Voss M, Larsen B, Leivuori M, et al. (2000) Stable isotope signals of eutrophication in Baltic Sea sediments. *Journal of Marine Systems* 25: 287–298.
- Voss M, Nausch G and Montoya J (1997) Nitrogen stable isotope dynamics in the central Baltic Sea: influence of deep-water renewal on the N-cycle changes. *Marine Ecology Progress Series* 158: 11–21.
- Wacker L, Němec M and Bourquin J (2010) A revolutionary graphitisation system: Fully automated, compact and simple. *Nuclear Instruments & Methods in Physics Research Section B, Beam Interactions With Materials and Atoms* 268: 931–934.
- Walker M, Head MJ, Berkelhammer M, et al. (2018) Formal ratification of the subdivision of the holocene Series/Epoch (Quaternary System/period): Two new global boundary stratotype sections and points (GSSPs) and three new stages/subseries. *Episodes* 41: 213–223.
- Waters CN, Turner SD, Zalasiewicz J, et al. (in submission) Candidate sites and other reference sections for the Global boundary Stratotype Section and Point (GSSP) of the Anthropocene series. *The Anthropocene Review*.
- Waters CN, Hajdas I, Jeandel C, et al. (2019) Artificial Radionuclide Fallout Signals. In: Zalasiewicz J, Waters CN, Williams M, et al. (eds) *The Anthropocene as a Geological Time Unit: A Guide to the Scientific Evidence and Current Debate*. Cambridge: Cambridge University Press, pp.192–199.
- Waters CN, Zalasiewicz J, Summerhayes C, et al. (2018) Global Boundary Stratotype Section and Point (GSSP) for the Anthropocene Series: Where and how to look for potential candidates. *Earth-Science Reviews* 178: 379–429.
- Zalasiewicz J, Waters CN, Ivar Do Sul JA, et al. (2016) The geological cycle of plastics and their use as a stratigraphic indicator of the Anthropocene. *Anthropocene* 13: 4–17.
- Zalasiewicz J, Waters CN, Summerhayes CP, et al. (2017) The Working Group on the Anthropocene: Summary of evidence and interim recommendations. *Anthropocene* 19: 55–60.
- Zalasiewicz J, Waters CN, Williams M, et al. (2019) *The Anthropocene as a Geological Time Unit: A Guide to the Scientific Evidence and Current Debate*. Cambridge: Cambridge University Press, p.361.
- Zillén L and Conley DJ (2010) Hypoxia and cyanobacteria blooms - are they really natural features of the late holocene history of the Baltic Sea? *Biogeosciences* 7: 2567–2580.